Geophysical insights into Tattapani Thermal Spring Azad Kashmir Pakistan: unravelling subsurface geology and geothermal potential

Mehboob Ur Rashid [1,2,3,*]
[1]*National Centre of Excellence in Geology University of Peshawar*
[2]*Geoscience Advance Research Labs, Geological Survey of Pakistan Islamabad*
[3]*Graduate School of Science and Engineering, Kagoshima University Japan*
**Corresponding author's email: mehboobgeo89@uop.edu.pk*
Submitted date: 26/03/2024 Accepted date: 15/05/2024 Published online: 05/06/2024

Abstract

Pakistan faces a growing energy demand, and thermal springs represent a potentially significant renewable energy source. This naturally heated thermal water can be harnessed for power generation, space heating and greenhouses, offering a renewable and sustainable alternative to fossil fuels. Pakistan possesses significant, yet underdeveloped, thermal potential and exploring and harnessing these resources could yield substantial environmental and economic benefits. The Tattapani thermal spring in Kotli, Azad Kashmir, is investigated for its geothermal energy potential due to its probable high temperatures, favourable geological conditions, and accessibility. The study aims to identify the subsurface geological structure, map the lithology, estimate the depth of the thermal spring reservoir, and infer the migration patterns of the thermal water. The resistivity profile of the Tattapani thermal spring unveiled five distinct layers exhibiting varying resistivity values. The uppermost layer, characterised by a high resistivity zone (> 500Ωm), corresponds to the dolomitic rock of the Abbottabad Formation. The second layer delineates lithological units of Murree sandstone, displaying resistivity values between >200Ωm and ≤500Ωm, indicative of potential meteoric freshwater. The third layer, marked by a resistivity range of >50Ωm to ≤200Ωm, signifies shaley to clayey lithology of the Patala Formation, indicating weathering and erosion by thermal fluid. The fourth layer corresponds to the migration of thermal plumes with a resistivity value of >25Ωm to ≤50Ωm, while a value of >05Ωm characterizes the fifth thermal spring layer of very low resistivity to ≤25Ωm. The very low resistivity values observed in the fifth layer are indicative of an anomalous zone, a characteristic feature of thermal springs. This low resistivity can be attributed to the high concentration of dissolved electrolytes within the mineral-rich thermal fluids. These fluids likely facilitate the alteration, weathering, and erosion of the surrounding rock formations, further enhancing the conductive nature of the zone. The Tattapani thermal spring exhibits a depth range of approximately 35-40 meters, increasing in the northeast-southwest (NE-SW) direction. Thermal plumes, primarily migrating in a NE-SW direction, have a depth range of about 25 meters. The VES data also delineates two aquifers: a shallow aquifer at approximately 10 meters depth and a deeper aquifer extending up to 20 meters, both hosted within the sandstone lithology. The shallow depth of the thermal plumes raises concerns about potential contamination of the deeper groundwater aquifer due to their overlapping depths. However, the presence of a barrier layer composed of shaley clay likely protects the shallow aquifer from current contamination. VES data revealed high-resistivity zones (dolomite) and low-resistivity zones (shale), consistent with Cambrian-Paleocene formations. The thermal spring is likely to emerge to the surface through a weak zone along the contact of shale and dolomite. A close correlation between the geological and resistivity sections suggests the presence of a fault or weak zone underlying the spring. This structure could facilitate a thermal convection cell, driving hot water upwelling and potentially sourced from the Poonch River. Detailed magnetic, gravity and geochemical surveys are recommended to portray the deep-seated structure of the Tattapani thermal spring while a geochemical survey will demarcate the contamination source by plume migration. Geothermometry and isotopic analysis are also recommended to show the subsurface temperature of thermal water.

Keywords: Geophysical investigation, Thermal spring, Resistivity structure, Lithological analysis, Vertical Electrical Sounding.

1. Introduction

Pakistan currently faces a critical power deficit, experiencing a shortage of 5000 Mega Watt (MW) with the demand increasing day by day factors by population growth and industrialisation (Raza et al., 2022; Awan and Sohail, 2023). The installed power capacity increased by 2.57% to 34,282 Mega Watt in 2019, while electricity generation grew by

2.1% to 87,324 GigaWatt hours (GWh) (Raza et al., 2022). However, this demonstrates a significant disparity, with power demand reaching a staggering 120,392 GWh in 2019 (Raza et al., 2022). This demand continues to rise at an annual rate of 9%, further exacerbating the challenges and causing widespread electricity shortages and power outages. To address the rising energy demand and ensure long-term sustainability, exploring alternative resources is crucial. Developing new, cost-effective options can significantly reduce reliance on finite fossil fuels and contribute to a more sustainable energy future (Shahid et al., 2020; Ahmad et al., 2022; Kanwal et al., 2022). Renewable energy resources are considered the optimal choice due to their cost-effectiveness in production, as well as their environmentally friendly nature, contributing to the achievement of Sustainable Development Goal 7 (SDG-7) (Holechek et al., 2022; Nastasi et al., 2022). Among renewable energy resources, geothermal energy stands out as a favourable option due to its cost-effectiveness and environmentally friendly attributes (Olabi et al., 2020; Lund and Toth, 2021). Pakistan is blessed with abundant geothermal resources, facilitated by favourable tectonic conditions, offering a promising avenue for sustainable energy exploration (Bakar, 1955; 1965; Shuja and Sheikh, 1983; Shuja and Khan, 1984; Shuja, 1986; Shuja, 1988; Todaka et al., 1988; Khan et al., 1999; Bakht, 2000; Zaigham et al., 2009; Ahmad and Rashid, 2010; Zaigham and Nayyar, 2010; Ahmad, 2014; Jamali et al., 2021). Pakistan boasts numerous geothermal zones with promising potential for efficient power generation if harnessed efficiently (Zaigham et al., 2009) (Fig. 1a). Thorough exploration and feasibility analysis of Pakistan's geothermal resources hold significant potential benefits for the nation, society, and regional development (Kaur et al., 2023; Yang et al., 2023). The Tattapani geothermal spring in Kotli, Azad Jammu and Kashmir (AJK), with its long-established reputation for hot thermal water, presents a compelling case study for further investigation (Todaka et al., 1988; Khan et al., 1999; Anees et al., 2015; Anees et al., 2017).

Geoelectrical methods find extensive applications in geophysical studies, primarily contributing to hydrology, subsurface mapping, and the delineation of geothermal resources (Yang et al., 2022; Bayowa et al., 2023; Oyeyemi et al., 2023; Rosado-Fuentes et al., 2023; Wang et al., 2024; Ahmed et al., 2024; Komori et al., 2024; Rashid et al., 2018). Currently, electrical resistivity imaging is regarded as the most effective technique for in-depth exploration of geothermal reservoirs (Ahmed et al., 2024; Komori et al., 2024; Wang et al., 2024). Resistivity imaging plays a crucial role in delineating subsurface lithology, cap rocks, hydrothermal alteration zones, and thermal water flows, offering maximum depth of penetration to characterize subsurface horizons (Dambly et al., 2024; Mohammed et al., 2024; Junaid et al., 2021; Rashid et al., 2017). The bulk resistivity of rocks is closely correlated with their fluid content, weathering signatures, rock type, porosity, and the type of water hosted in the rock (Yanis et al., 2022; Akpan et al., 2023; Fu et al., 2024). Geothermal resources are identifiable through lower resistivity values compared to surrounding rocks, attributed to elevated dissolved salt (chlorides) content (Pavić et al., 2023; Ashadi et al., 2024). This high concentration of dissolved ions, causes resistivity values to decrease significantly, by up to two orders of magnitude compared to cold water or typical rock-forming minerals (Jamali et al., 2021; Komori et al., 2024; Wang et al., 2024).

The study area is located between 73°52′ and 74°00′ east longitude and 33°30′ and 33°46′ north latitude according to Survey of Pakistan topographic sheet No. 43-G/14. The Tattapani spring primarily emerges along the left bank of the Poonch River, with its outpouring on the right bank obstructed by fluvial sediment deposits resulting in overflows by river Poonch. This study aims to utilize geophysical surveys for subsurface mapping of potential geothermal reservoirs of Tattapani. These findings will be crucial for identifying optimal locations for future geothermal well drilling and feasibility analyses, ultimately enhancing the potential for successful geothermal resource development.

2. Geological setting

The study area is situated within the sub-Himalayan region folded to imbricate thrust

faults, characterized by the exposure of lithological units from the Precambrian to the Miocene age (Shah et al., 2007; Thakur et al., 2010). The oldest exposed rocks in the area belong to the Cambrian-aged Abbottabad Formation (Shah et al., 2007) (Fig. 1b). The Abbottabad Formation consists of cherty dolomite in its lower section, transitioning upwards into fine-grained quartzite. The Abbottabad Formation is unconformably overlain by the Paleocene Patala Formation, which is dominated by shale (Shah et al., 2007). The thermal spring of Tattapani is primarily sited at the northern apex of the Tattapani anticline (Fig. 1c). It is bounded by the Patala Formation and Murree Formation, featuring a faulted contact juxtaposed with the Abbottabad and Patala Formation (Shah et al., 2007; Thakur et al., 2010).

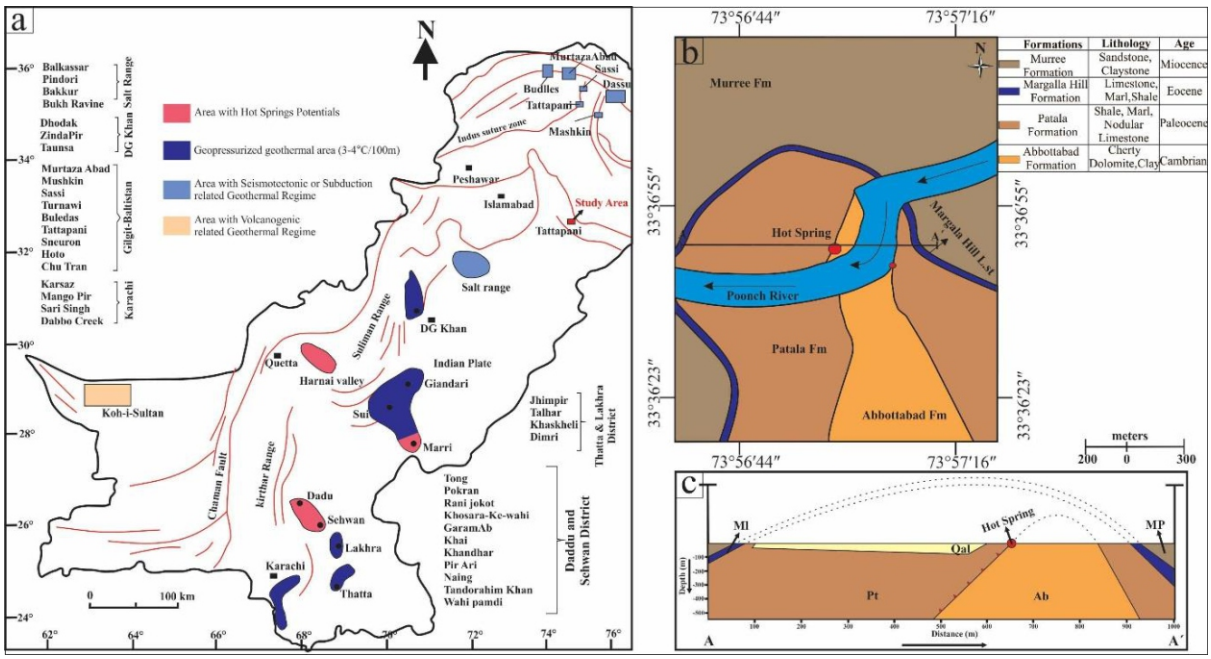

Fig. 1. (a) Geothermal Map of Pakistan showing thermal spring Pakistan (Zaigham et al., 2009), b) Geological Map of Tattapani Thermal Spring (Shah et al., 2007), c) Geological Cross section along Tattapani Thermal Spring (Shah et al., 2007).

3. Materials and methods

A 2D electrical survey was carried out along the thermal spring of Tattapani in Kotli, AJK, utilizing the Schlumberger electrode configuration with the generation of four 2D profiles adjacent to the thermal spring (Fig. 2a). The survey employed a total of 21 vertical electrical soundings (VES) arranged in a collinear fashion to generate these 2D profiles. The survey design was optimized for the available space and accessibility constraints to achieve comprehensive coverage of the target area. The acquisition of data for the vertical electrical soundings (VES) employed a TSQ-3 transmitter and RDC-10 receiver from Scintrex (Canada), along with a generator and its associated ancillary equipment (Fig. 2b). The transmitter operates with an input voltage of 220 volts and an output voltage ranging from 300 to 1500 volts, with a current range of 0.1 to 10 amperes, within a time domain of 2 seconds. The RDC-10 receiver operates within the same 2-second time domain and averages 15 readings per cycle, boasting a measurement reliability of 0.1 Ωm. The Schlumberger electrode configuration was adopted for data acquisition, employing a potential electrode (MN) spacing range of 4 meters to 50 meters and a current electrode (AB/2) spacing range of 6 meters to 500 meters (Fig. 2c). The Schlumberger electrode configuration was chosen due to its well-established capability of achieving greater depth of investigation and improved vertical resolution for a given electrode separation separation (Loke et al.,

2020). In the Schlumberger VES survey, , the spacing of current electrodes (AB/2) was progressively increased to acquire a maximum depth of investigation (Telford et al., 1990; Joshua et al., 2011; Loke et al., 2020). The Scintrex TSQ-3 transmitter generates electrical pulses in the time domain with a cycle time of 2 seconds. During each cycle, the RDC-10 receiver acquires and averages 15 readings, resulting in a single data point representing the average apparent resistivity. The apparent resistivity data are presented in the form of sounding curves, which are then subject to both qualitative and quantitative interpretation. The apparent resistivity values obtained during the fieldwork are plotted on a bi-logarithmic scale, with electrode spacing and apparent resistivity values on the x- and y-axis respectively. The data analysis is performed using the IPI2win software, which employs inversion techniques adopting curve fitting techniques to classify the apparent resistivity curves into different layers, determining the corresponding thickness, depth, and true resistivity for each layer (Bobachev, 2002). The input parameters for the software include the apparent resistivity values recorded during the survey, as well as the separation distances between the current and potential electrodes (MN and AB). This interpretation aims to differentiate the data based on the contrast in resistivity values, isolating them into various subsurface lithology's using the standard resistivity range of different lithological units (Telford et al., 1990) (Fig. 3). For each collinear VES profile, 1D geoelectrical sections were generated using software (IPI2win) to depict the variation of true resistivity with depth, corresponding to the inferred lithological changes (Fig. 4). The Iso-resistivity maps were constructed at specific depths (10 m, 20 m, 60 m, 80 m, 100 m and 200 m) to depict the lateral distribution of resistivity at each chosen depth, potentially reflecting variations in lithological properties (Fig. 5). The 1D sections were integrated to create a comprehensive 2D true resistivity model for each profile, illustrating the lateral and vertical variations in resistivity, associated with different subsurface lithology's (Fig. 6). Statistical Distribution Curves (SDCs) were generated for apparent resistivity along each profile. These SDCs provide insights into the central tendency (mean) and variation (spread) of the resistivity values within each profile (Fig. 7). The Dar Zarrouk parameters, a set of electrical resistivity values derived from vertical electrical sounding (VES) data, are used to characterize aquifer properties such as permeability, hydraulic conductivity, aquifer thickness, and freshwater potential (Iduma and Uko, 2016; Kazakis et al., 2016; Mahmud et al., 2022; Ewusi et al., 2024). This study employs the Dar Zarrouk parameters to analyze the Tattapani thermal spring, investigating its transverse unit resistivity, longitudinal conductance, and macro anisotropy (Fig. 8).

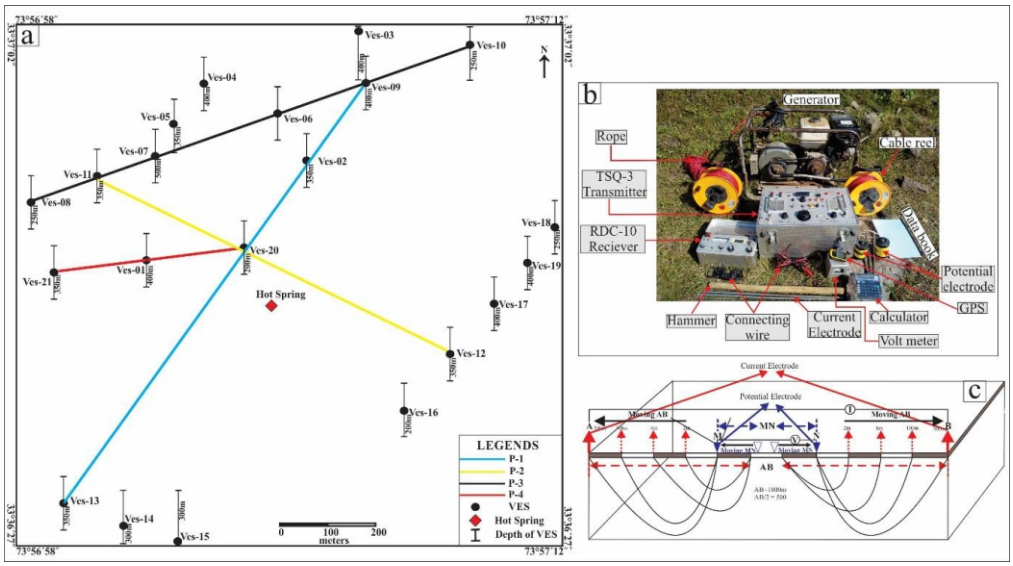

Fig. 2. a) Base Map of the resistivity showing location VES and 2D profiles, b) Instrumentation utilized for resistivity survey along Tattapani thermal spring, c) Schematic diagram of Schlumberger electrode configuration.

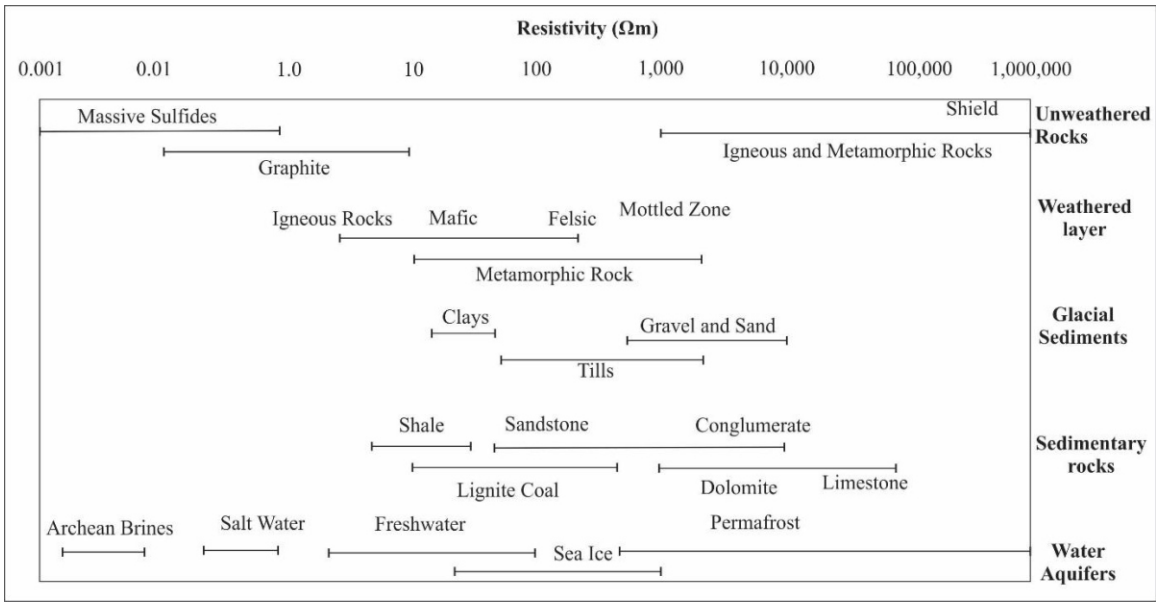

Fig. 3. Standard resistivity values of different geological materials (Telford et al., 1990).

3. Results

4.1 Geo-electric sections

Geoelectrical sections were constructed for each of the 12 Vertical Electrical Sounding (VES) locations along the four 2D profiles (Fig. 4). These sections were generated by interpreting the variations in apparent resistivity, which are likely linked to the contrasting electrical properties of different subsurface lithology (Telford et al., 1990) (Fig. 3). Interpretation of the geoelectrical sections represents four distinct lithological that are delineated to a maximum depth of 500 meters. These units, identified based on their resistivity characteristics, likely correspond to dolomite, sandstone, shale, and clay. The very low resistivity anomalies indicative of potential thermal plumes or a thermal spring were identified (Singh et al., 2021; Finn et al., 2022) (Fig. 4). The geoelectrical lithological section revealed that the topmost soil is mostly dolomitic in composition with some shale and clay along VES 10, 12 and 13. As depth increases, the dolomite sequence is underlain by shale, clay and sandstone representing the lithology of different formations. The sandstone is the favourable perennial water-bearing horizon in the Tattapani area, with depths reaching from 10 meters to 100 meters. Two aquifers are delineated the shallow one is encountered at a depth of 10 meters (VES-02, and 20) while the deeper one is encountered at a depth of 20 meters (VES-13). The shallow aquifer is in contact with the dolomitic lithology, while the deeper one is with the shaley clay lithology. The thermal plumes reach a very shallow depth of 25 meters (VES-02), inferring contamination of the deeper aquifers, while the thermal spring is encountered with a depth of 40 meters (VES-20). The interpretation of the geoelectrical sections suggests a potential vulnerability of the deeper permanent water aquifer to contamination by the identified thermal plumes, owing to their relatively shallow depth. Due to the shallow origin and continuous mixing with the surrounding aquifer, the thermal spring water cools progressively as it rises to the surface. This impedes the determination of the true subsurface reservoir temperature of the Tattapani thermal spring. The high surface temperature of the Tattapani Spring, reaching approximately 60°C, suggests a potentially elevated subsurface reservoir temperature (Anees et al., 2015; 2017). As the thermal water ascends through the subsurface, it likely mixes with shallower and deeper groundwater, gradually lowering its temperature before reaching the surface (Bouaicha et al., 2019; Dávalos-Elizondo et al., 2021).

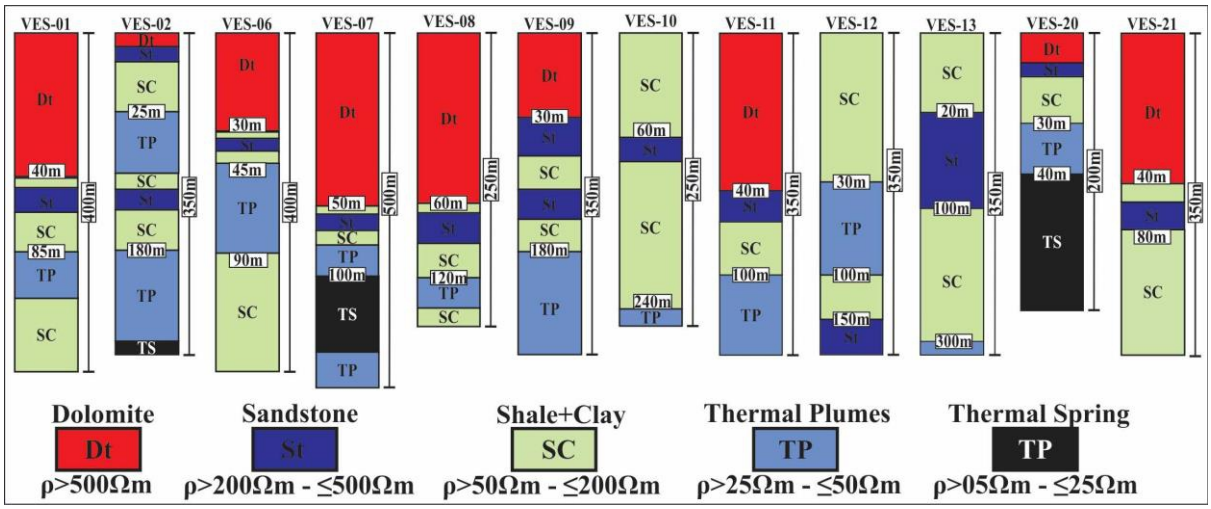

Fig. 4. Geoelectrical section of twelve VES stacked along four 2D profiles.

4.2 Iso-resistivity maps

To understand the subsurface resistivity variations within the study area, iso-resistivity maps are generated at depths of 10 m, 20 m, 60 m, 100 m, and 200 m (Fig. 5). These maps categorize resistivity zones based on magnitude: high (> 300 Ωm), moderately high (100-200 Ωm), moderately low (50-100 Ωm), and very low (< 50 Ωm). For a more comprehensive interpretation of the geothermal conditions, low-resistivity formations are identified within the iso-resistivity maps using a distinct attribute (Jamali et al., 2021; Singh et al., 2021; Komori et al., 2024). At a depth of 10m most of the area is covered by high resistivity values in the range of 300Ωm to 800Ωm representing high resistivity dolomite of Abbottabad Formation. Moderate to high resistivity values in dolomite are primarily controlled by low water saturation, limited alteration by thermal fluids, and a relatively intact pore structure (Jabrane et al., 2023). The Tattapani thermal spring is situated at the intersection of a high-low resistivity zone trending northeast (NE) along the right bank of the Poonch River. The low resistivity values, down to 100Ωm, suggest the presence of a shale and clayey lithology belonging to the Patala formation. This formation is interpreted to be in thrust contact with the Abbottabad Formation, potentially forming the Tattapani anticline (Mughal et al., 2004; Shah et al., 2007). This zone exhibits a decrease in resistivity value with increasing depth. At a depth of 20 m, the resistivity drops to a range of 20Ωm-100Ωm, consistent with a transition to shale or clay lithology, as supported by the geological section at this depth (Shah et al., 2007). The shale and clay formations typically have low resistivity values, down to 100Ωm, due to their high porosity and the presence of conductive pore water, making them good electrical conductors (Krzyżak et al., 2020; Escobedo et al., 2021). At a depth of 60 m, a low-resistivity anomaly ranging from 20Ωm to 60Ωm is identified along a north-south (NS) trending, narrow zone. This anomaly is interpreted as indicative of hot water springs and associated hydrothermal alteration, which can decrease resistivity values in the rock (Zhu et al., 2022; Komori et al., 2024). With increasing depth, the low-resistivity anomaly zones expand, suggesting intensified hot water alteration and potentially a deeper extent of the hot water resource (Zhu et al., 2022). The thermal water alteration can significantly decrease the resistivity of surrounding rocks (Escobedo et al., 2021). This process primarily alters the mineral composition and pore water characteristics, but may also indirectly induce weathering and erosion, further contributing to the overall decrease in resistivity (Ladygin et al., 2014; Wang et al., 2024). At greater depths, the anomalous zone extends in both northeast (NE) and northwest (NW) directions, illustrating the maximum extension of the geothermal resource at deeper levels. At greater depths (100m & 200m), a high resistivity anomaly with significant values (>300Ωm) is

concentrated in the northeast side of the Iso-resistivity section. The high-resistivity zone, interpreted as dolomitic lithology, potentially represents a thrust horizon. This interpretation is based on the observation of lower resistivity rocks situated above the dolomite at shallower depths, possibly indicating a thrust sequence. The reappearance of dolomite at greater depths could further support this thrusting scenario (Cheon et al., 2023). The iso-resistivity map, constructed based on resistivity variations with depth, reveals the presence of very low resistivity anomaly zones starting from 60 meters and extending deeper. Integration with resistivity sections and the statistical distribution curve (SDC) further strengthens the validation of the iso-resistivity map.

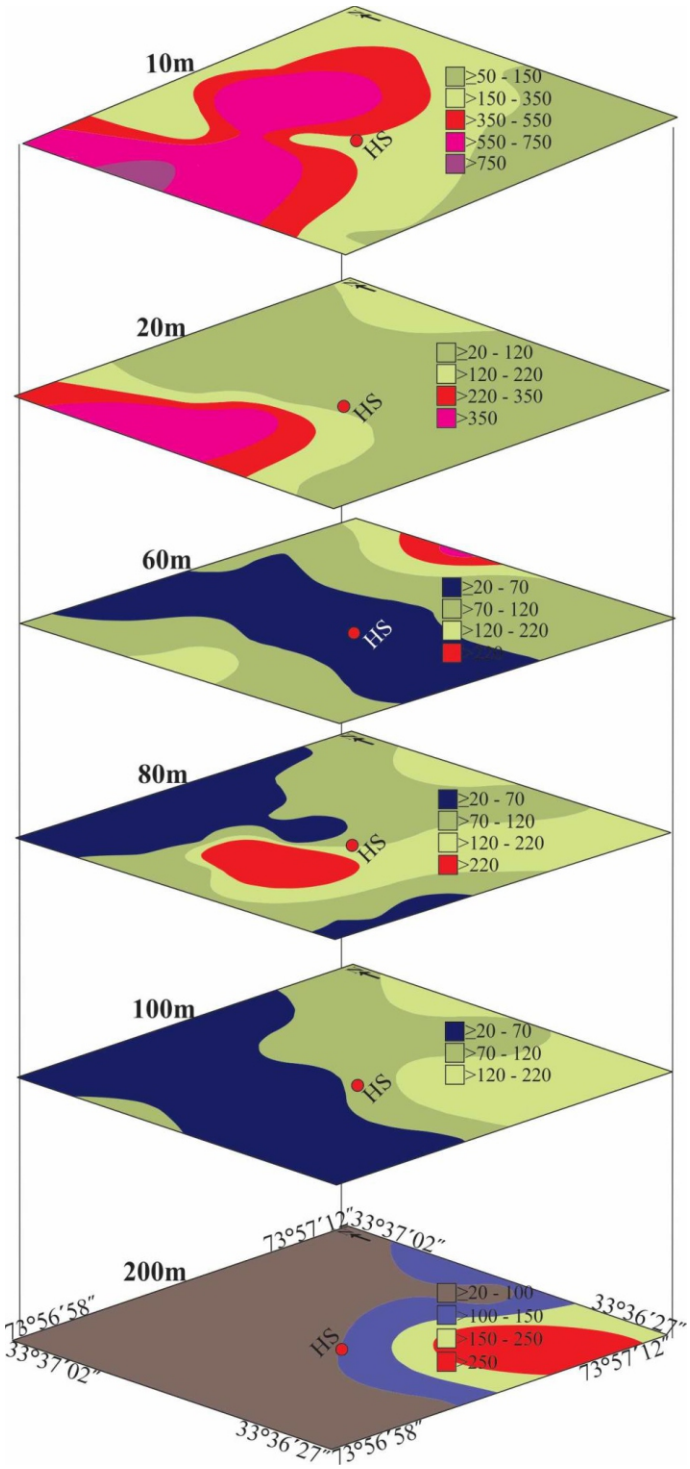

Fig. 5. Iso resistivity map of all 21 VES at a depth interval of 10, 20, 60, 80,100 and 200 meters.

4.3 Resistivity section

The 2D resistivity section was generated for the VES profiles, specifically focusing on points that are either collinear or approximately collinear (Fig. 6). This methodology was employed to create resistivity sections effectively portraying the variation in resistivity across selected points within a profile (Araffa et al., 2015; Abdulkadir and Eritro, 2017; Singh et al., 2021). The resulting resistivity section delineates four distinct resistivity zones categorized by resistivity contrast: a very low resistivity zone indicative of a thermal spring (>05Ωm - ≤25Ωm), a low zone associated with thermal plumes (>25Ωm - ≤100Ωm), a moderate zone representing shale and clay (>100Ωm - ≤200Ωm), and a high zone corresponding to sandstone (>200Ωm – ≤500Ωm) and a very high zone associated with dolomite (>500Ωm). This categorization facilitates the interpretation of resistivity variation across profile points, offering valuable insights into subsurface resistivity distribution. Profile-I, oriented along the SW-NE direction, spans a total length of 1.3km and a depth of 500m. It reveals the lithological distribution of dolomite, sandstone, shale, clay, thermal plumes, and thermal springs. The profile indicates a thermal spring in the depth range of 45m to 250m, characterized by a very low resistivity of 20Ωm. The resistivity signature suggests that thermal plumes originating from the spring migrate in both SW and NE directions. Profile-I further reveals the presence of a thermal spring on the NE side, exceeding a depth of 300 m. This finding suggests a potential direction of lateral flow or extension of the geothermal system. The shallower thermal spring (45-250 m) resides beneath a sequence of less permeable shale and clay formations, which may act as a cap, confining the geothermal fluids. Overlying the shale and clay is a layer of sandstone, potentially serving as a perennial freshwater resource. The uppermost layer is interpreted as dolomite, capping the entire geological sequence profile-II, oriented along NW-SE, spans 900m in total length and a depth range of 300m, displaying a lithological sequence similar to profile-I. Profile-II identifies a thermal spring zone at a depth of approximately 80 meters, extending in an NW-SE direction. The spring appears to be situated within a freshwater zone encompassed by a sandstone unit within a depth range of 10-50 meters. This unit is capped by dolomitic lithology at the top and underlain by shale and clay formations at the bottom. Profile-III, a SE-NW trending geoelectrical profile, extends for 1100 meters and reaches a depth of 500 meters. This profile reveals a thermal spring zone at a depth of approximately 100 meters. The associated thermal plumes migrate NW along the identified shale/clay unit. The shallow thermal plumes are also detected at a depth of around 30 meters along profiles VES-02, 12, and 20. These shallow plumes may pose a potential threat of contaminating freshwater resources (Navarro et al., 2011). The deeper portion of the thermal spring system appears to be located along the NE side at a depth range of 400 meters. The cap rocks overlying the geological sequence consist of dolomite at the top, followed by sandstone and then shale to clay at the bottom. Profile-IV, oriented SW-NE, extends for 500 meters and reaches a depth of 400 meters. This profile depicts a shallow thermal spring zone at approximately 40 meters depth on the NE side. The thermal plumes appear to trend towards the SW, raising concerns about potential freshwater contamination. The 2D resistivity section portrays the thermal spring system at various depths. At shallow depths (40-100 meters), a zone of thermal influence is observed, while deeper zones exceeding 300 meters also exhibit thermal signatures. The overall trend of the thermal spring system is along the NE side, with associated plumes migrating in an NE-SW direction. The shallow thermal plumes detected at depths of 25-30 meters pose a potential threat of contaminating freshwater resources. The freshwater zone itself appears to be encompassed by a sandstone unit at depths of 20-30 meters. The geological cross-section further reveals that the hot spring originates at the contact zone between dolomite and shaley clay lithology (Shah et al., 2007). While a barrier zone of shaley clay might hinder plume migration in some areas (Krzyżak et al., 2020). The presence of an inferred faulted contact between the dolomite and shaley clay formations provides a vent for the thermal spring to emerge (Zhou et al., 2023).

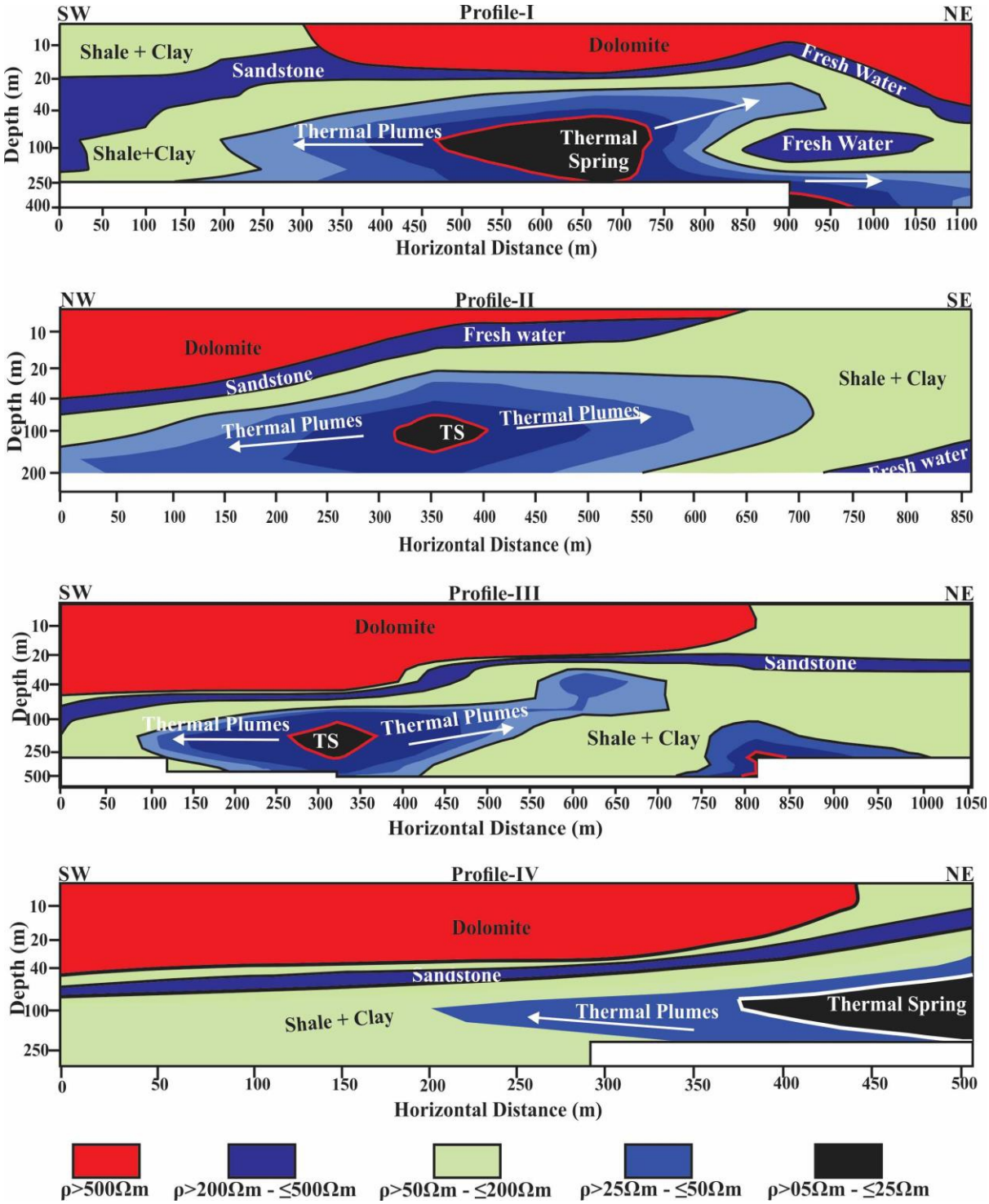

Fig. 6. 2D resistivity section of Tattapani thermal spring along four profiles.

5. Statistical distribution of apparent resistivity

Statistical Distribution Curves (SDCs) of apparent resistivity were generated using IPI2win software to analyze the average resistivity variations across each profile (Profile I-IV). These curves reveal a consistent resistivity trend across the profiles, followed by a significant decrease in resistivity from the surface, as illustrated in Fig. 7. Anomalous low-resistivity zones (20Ωm - 50Ωm), indicative of thermal springs, are identified at varying depths in each profile: : 60 m for Profile I, 80 m for Profile II, 150 m for profile III, and 65 m for profile IV. The overall sequence identified by

the SDC is dolomite (top layer), followed by shale/clay, sandstone, thermal plumes, and finally, the thermal spring. This layering aligns well with the observations from the geoelectrical sections and resistivity profiles. The SDCs effectively portray the presence of shallow and deeper aquifers along each profile. The proximity of thermal plumes to the aquifer horizons, as depicted by the SDCs, highlights the potential risk of contamination. The consistent trend observed in the SDCs aligns with the findings from the resistivity sections, geoelectrical sections, iso-resistivity curves, and the established geological characteristics of the area.

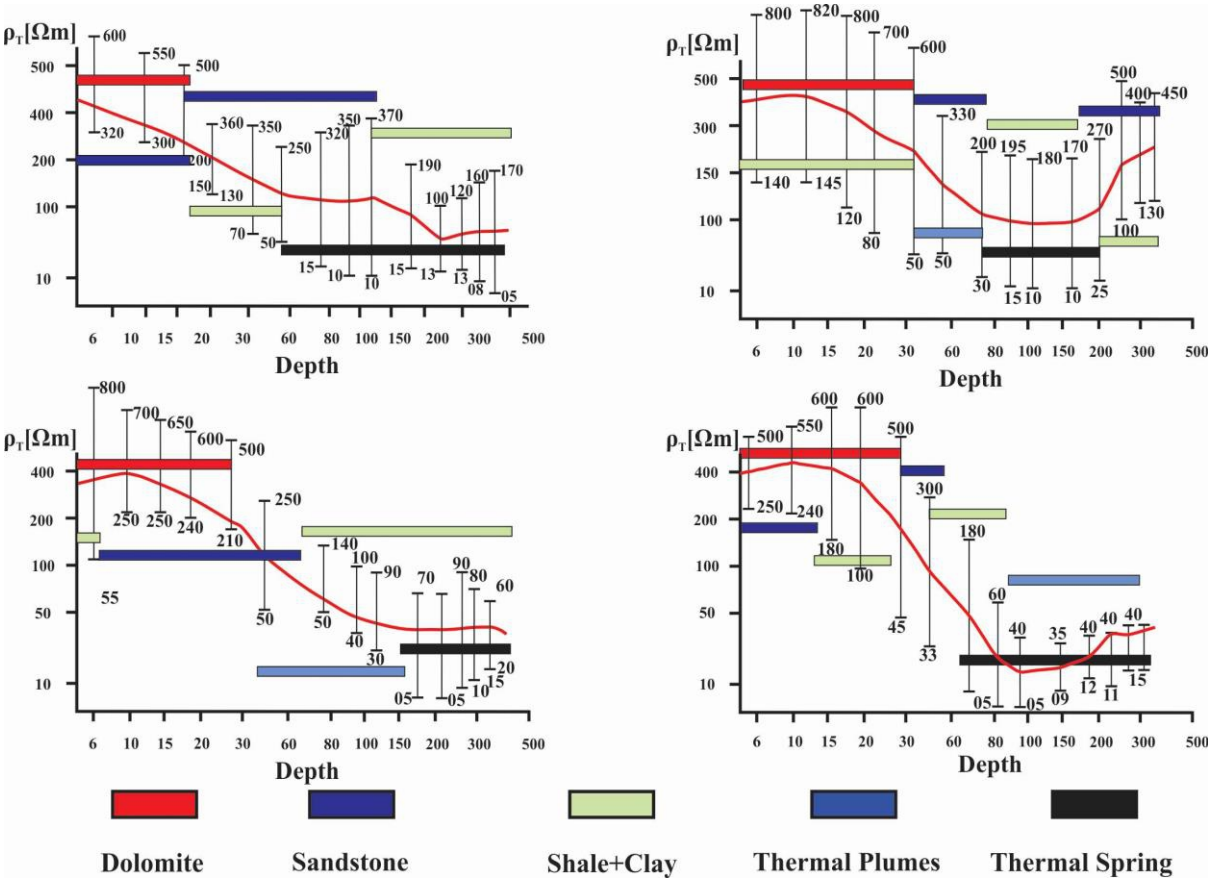

Fig. 7. Statistical Distribution of resistivity along four 2D profiles.

6. Dar Zarrouk parameters of hydraulic conductivity

The relationship between hydraulic conductivity (K) and electrical conductivity (EC) has been explored by previous researchers, particularly in the context of water quality assessment (Batayneh, 2013; Iduma and Uko, 2016; Kazakis et al., 2016; Mahmud et al., 2022). This link between K and EC holds significant importance for water quality studies. Two crucial parameters used to describe the conductivity of geological media are longitudinal unit conductance (S) and transverse unit resistivity (TR), which collectively contribute to macro anisotropy, as defined by Dar Zarrouk Parameters (DZP) as highlighted by Maillet (1947). Geological materials characterized by high longitudinal conductance (S) and transverse unit resistance are indicative of high recharge capacity and are often considered prime locations for water exploration, as discussed by Iduma and Uko (2016). Maps depicting transverse unit resistance and longitudinal unit conductance are generated for the study area to provide insights into the recharge capabilities of the geological formations, thereby facilitating the understanding of thermal plume flow patterns (Fig. 8). The average total transverse unit resistance values range from 20 to 300Ωm (Fig. 8a). The general trend of transverse unit

resistivity (TR) demonstrates an increase towards the NE and SW sides of the study area, promoting the flow of thermal plumes. Minimal TR values, ranging from 20 to 40Ωm, are recorded along specific VES points such as VES-20, 13, and 05. The low TR values observed along VES-20 are attributed to rock alteration by hot plumes, rendering them more permeable and conductive (Markússon and Stefánsson, 20111 Ladygin et al., 2014). Conversely, the NE side exhibits higher TR values within the range of 140 - 300Ωm. Analysis of the TR map suggests the presence of permeable layers on both the NE and SW sides, facilitating the flow of thermal water (Ewusi et al., 2024). Total longitudinal conductance (S) serves as a geoelectrical parameter to delineate areas of groundwater potential based on unit resistivity over a known thickness (Kazakis et al., 2016). Areas characterized by high S values typically indicate a relatively thick conductive succession with good porosity (Mahmud et al., 2022). In the study area, S values vary between 0.95 and 15 mohos (Fig. 8b), with higher values (6-15 mohos) observed in the north-western side, indicative of more permeable beds. Moderate S values (2-5 mohos) are observed on the SW side, while lower values (0.95-2 mohos) are found on the NE-SE side, suggesting the presence of porous beds such as shale and clays. A macro-anisotropy map was generated, revealing values ranging from 1 to 2.7 (Fig. 8c). This map helps to elucidate significant variations in the lithological fabric surrounding the hot spring. The identified anisotropy pattern suggests potential fault orientations in a NE-SW direction, which aligns with the interpretations from the geological sections and resistivity profiles.

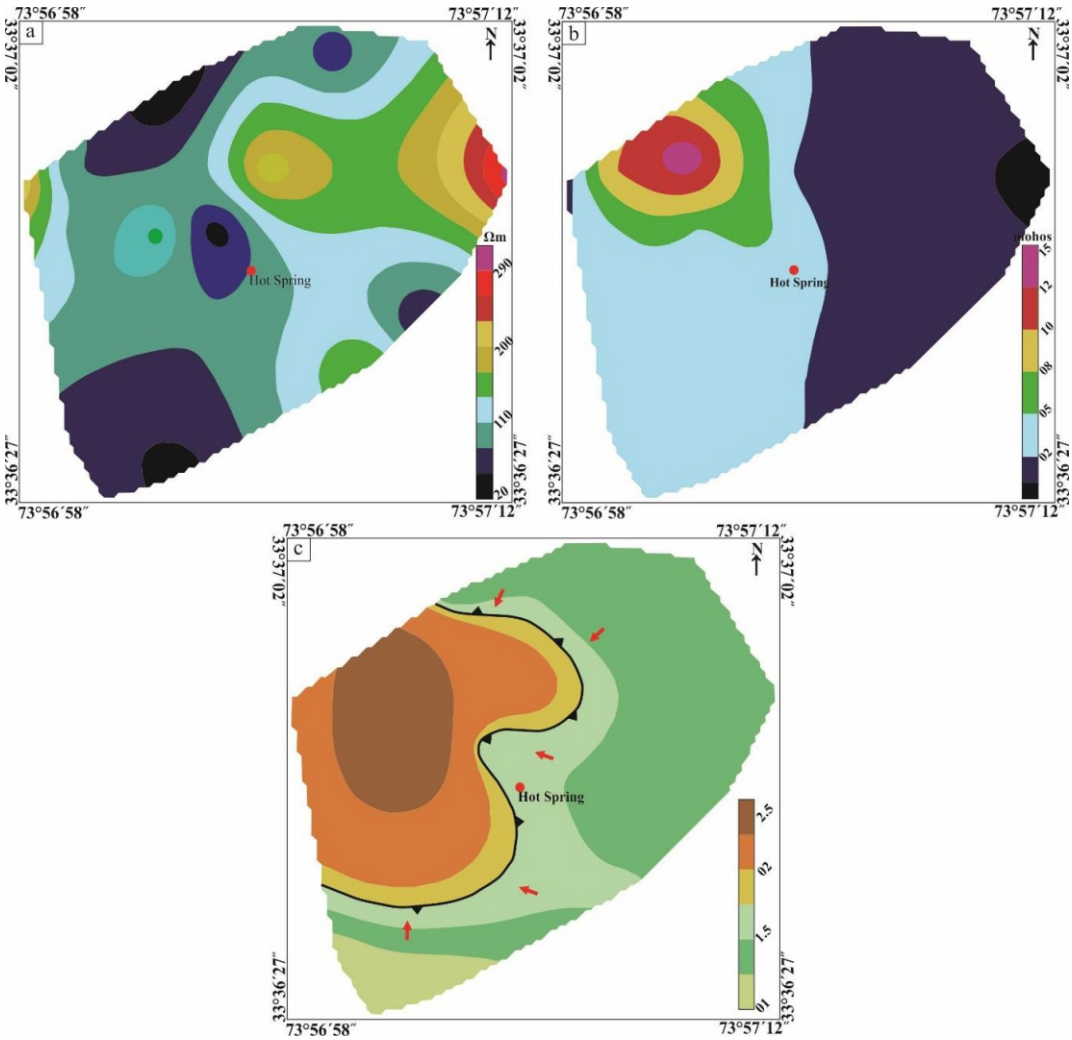

Fig. 8. Dar Zarrouk Hydraulic parameters of Tattapani Thermal Spring, a) Transverse unit resistivity, b) Longitudinal conductance, c) Macro anisotropy.

7. Discussion

Generally, reservoir rocks of geothermal origin typically exhibit anomalies with low resistivity due to the change by high mineral content and geothermal water (Komori et al., 2024). In the case of the thermal spring of Tattapani, rocks with low resistivity are found beneath high-resistivity rocks at greater depths, indicating mineral alteration by hydrothermal water (Todaka et al., 1988; Anees et al., 2015; Rashid and Anwar, 2018). The hydrothermal alteration is indicated by the alkaline nature (pH 6.62 to 6.65) of Tattapani thermal water, classifying it as an HCO3 type (Anees et al., 2015). The alkaline nature of the water tends to erode the surrounding rock which is mostly dolomite (Fig. 1b), resulting in the presence of HCO-3-type water (Ladygin et al., 2014). The erosion and leaching by the alkaline thermal water of Tattapani thermal spring enhance the dissolved mineral content of the water, resulting in a drop in resistivity and increased conductivity (Finn et al., 2022). The effect of thermal plumes is also evident as the thermal water migrates and comes into contact with fresh water, resulting in the formation of thermal plumes characterized by low resistivity (Singh et al., 2021). These observed resistivity structures result from mineral alteration, erosion and leaching by alkaline hydrothermal water resulting in a drop in resistivity (Abdulkadir and Eritro, 2017; Chabaane et al., 2017). The analysis identifies anomalous zones of low resistivity through Vertical Electrical Sounding (VES) mapping, reflected in geoelectrical sections, Resistivity sections, and Iso-resistivity maps (Figs. 4 to 8). All the resistivity sections consistently depict high resistivity values at the surface, typically exceeding 200Ωm (apparent resistivity) and potentially reaching even higher >500Ωm true resistivity values (Fig. 6). This observation strongly suggests a dolomitic composition for the surficial sedimentary cover rock (Jabrane et al., 2023). Shale to shaley clayey lithology is present in certain geoelectrical sections (e.g., VES-02, 03, 05, and 04), attributed to rock alteration and weathering (Escobedo et al., 2021; Ladygin et al., 2014) (Fig. 4). The resistivity sections identify very low resistivity zones (05Ωm - 50Ωm) that are indicative of geothermal manifestations with moderate to low degrees of hydrothermal alteration (Jamali et al., 2021; Komori et al., 2024; Nieto et al., 2019; Singh et al., 2021) (Fig. 6). The low-resistivity anomaly along Profile I extends in the SE-NE direction, indicating the presence of low-temperature minerals such as smectite and zeolite (Singh et al., 2021) (Fig. 6). These minerals are commonly associated with relatively low-temperature hydrothermal alteration caused by the Tattapani thermal water interacting with the surrounding shaley clay unit (Escobedo et al., 2021). The data indicates that the depth of the geothermal spring ranges from about 35 to 40 meters, with an increase in depth observed in the NE – SW direction (Fig. 4). The mixing of thermal water with fresh water is clearly depicted by the 2D resistivity section, illustrating the migration of thermal plumes (Fig. 6). Two groundwater aquifers are delineated by both the geoelectrical and resistivity sections: a shallow aquifer at approximately 10 meters depth and a deeper aquifer extending from about 20 meters to 50 meters depth (Fig. 4). The shallow aquifer remains uncontaminated and pure, serving as the sole source of drinking water in the study area. In contrast, the deeper aquifer is contaminated by thermal plumes, with its effects visibly impacting the local community. The migration of fluids is impeded by the less permeable layer of shaley clay, preventing further contamination of the shallow aquifer (Krzyżak et al., 2020). The geothermal anomaly is inferred to migrate in the NW and NE directions, with a dominant trend toward the NE side (Figs. 5 and 6). The migration of thermal plumes poses a significant threat to groundwater quality due to the mobilization of contaminants and alteration by geochemical processes (Dotsika et al., 2006; Aksoy et al., 2009; Navarro et al., 2011; Bayowa et al., 2023). However, determining the correct geothermal temperature by collecting surface water is not feasible due to the mixing of thermal water with fresh water (Fig. 6). Such mixing can contaminate the thermal signature and compromise the accuracy of temperature measurements (Bouaicha et al., 2019; Dávalos-Elizondo et al., 2021). Therefore, portraying the actual subsurface temperature correctly through geothermometry is challenging. The resistivity and geological data are in agreement indicating the presence of the thermal spring

along a contact zone of high-resistivity dolomite with low-resistivity shale oozing along the contact of these contrasting lithology.

8. Conclusions

Geophysical investigations using Vertical Electrical Soundings (VES) in the Tattapani thermal spring area, along with analysis of geoelectrical sections and resistivity profiles maps, provided valuable insights into the subsurface geology and geothermal potential. The overall trend of mean resistivity decreases downward, sharply dropping to 05Ωm showing a thermal spring of low resistivity. The hot, alkaline water from the thermal spring likely weathers the surrounding rock, dissolving minerals and altering pore water chemistry. This process lowers the rock's resistivity, making it more conductive. The VES surveys identified the Tattapani thermal springs based on low resistivity, indicating a minimum depth of 35-40 meters for the springs. The overall depth of the springs increases in an NW-SW direction and may potentially exceed 300 meters. The shallow thermal plumes, characterized by resistivity values ranging from 25Ωm to 50Ωm, were detected at a depth of approximately 25 meters and exhibited migration in an NE-SW direction. Resistivity surveys identified the presence of two freshwater aquifers at depths of 10 and 20 meters. These aquifers exhibit low to moderate resistivity values (200Ωm - 500Ωm) and are likely hosted within sandstone lithological units, suggesting the presence of cold meteoric water. The ascent of hot water towards the surface presents a potential risk of thermal plume and deep aquifer water mixing. This overlap in their depth ranges (around 25 meters for plumes and 10-20 meters for aquifers) could lead to a reduction in surface water temperature and, more importantly, possible contamination of the deeper freshwater resources. The ascent of hot water appears to be facilitated by a weak zone along the faulted contact between the Cambrian Abbottabad Formation (dolomite) and the overlying Paleocene Patala Formation (shale). This weaker zone probably a faulting is strong evidence of the geologic forces that shaped the area, potentially contributing to the formation of the Tattapani anticlinal structure. The potential for deep aquifer contamination by thermal water due to possible mixing during ascent is a significant concern. This contamination could render the freshwater resources unsuitable for drinking and necessitates further detailed studies to assess the risk and develop mitigation strategies. However, the combined analysis of tectonic structures and the identified thermal system suggests a promising location for establishing a pilot geothermal power plant. Confirmation of this potential would require integrated geophysical (gravity, magnetic) and geochemical surveys to fully characterize the geothermal reservoir and ensure environmental sustainability.

Acknowledgement

This research is part of a PhD research undertaken at the National Centre of Excellence in Geology, University of Peshawar. The research work is funded by the Geoscience Advance Research Laboratories (GARL) Geological Survey of Pakistan (GSP) Islamabad for the execution of geophysical studies at Tattapani.

Authors Contributions

Mehboob ur Rashid proposed the main concept and was involved in the write-up of the manuscript, collected field data, conducted the relevant literature review, prepared illustrations and plates of figures and proofread the manuscript.

Conflict of Interest

All authors declare no conflict of interest.

Data Availability Statement

The data sets generated and analysed during the current study are available in the main body of the paper.

References

Abdulkadir, Y. A.; Eritro, T. H., 2017. 2D resistivity imaging and magnetic survey for characterization of thermal springs: A case study of Gergedi thermal springs in the northwest of Wonji, Main Ethiopian Rift, Ethiopia. Journal of African Earth

Sciences, 133, 95-103.
Ahmad, I.; Rashid, A., 2010. Study of geothermal energy resources of Pakistan for electric power generation. Energy Sources, Part A: Recovery, Utilization, and Environmental Effects, 32(9), 826-838.
Ahmad, J., 2014. The Geothermal Energy Potential of Pakistan Clean Sustainable Solution for Our Energy Future. GRC Transactions, 38, 571-576.
Ahmad, U. S.; Usman, M.; Hussain, S.; Jahanger, A.; Abrar, M., 2022. Determinants of renewable energy sources in Pakistan: An overview. Environmental Science and Pollution Research, 29(19), 29183-29201.
Ahmed, I.; Liu, H.; Chen, R.; Ahmad, J.; Shah, S. A.; Fahad, S.; Rahim, O. A.; Ullah, F.; Rui, L., 2024. Geothermal Resource Exploration in Reshi Town by Integrated Geophysical Methods. Energies, 17(4), 856.
Akpan, A. E.; Ekwok, S. E.; Ben, U. C.; Ebong, E. D.; Thomas, J. E.; Ekanem, A. M.; George, N. J.; Abdelrahman, K.; Fnais, M. S.; Eldosouky, A. M., 2023. Direct detection of groundwater accumulation zones in Saprock Aquifers in tectono-thermal environments. Water, 15(22), 3946.
Aksoy, N.; Şimşek, C.; Gunduz, O., 2009. Groundwater contamination mechanism in a geothermal field: a case study of Balcova, Turkey. Journal of Contaminant Hydrology, 103(1-2), 13-28.
Anees, M.; Shah, M. M.; Qureshi, A.; Manzoor, S., 2017. Multi proxy approach to evaluate and delineate the potential of hot springs in the Kotli District (Kashmir, Pakistan). Geologica Acta, 15(3), 0217-0230.
Anees, M.; Shah, M. M.; Qureshi, A. A., 2015. Isotope studies and chemical investigations of Tattapani hot springs in Kotli (Kashmir, NE Pakistan): Implications on reservoir origin and temperature. Procedia Earth and Planetary Science, 13, 291-295.
Araffa, S. A. S.; Helaly, A. S.; Khozium, A.; Lala, A. M.; Soliman, S. A.; Hassan, N. M., 2015. Delineating groundwater and subsurface structures by using 2D resistivity, gravity and 3D magnetic data interpretation around Cairo–Belbies Desert road, Egypt. NRIAG Journal of Astronomy and Geophysics, 4(1), 134-146.
Ashadi, A. L.; Tezkan, B.; Yogeshwar, P.; Hanstein, T.; Kirmizakis, P.; Khogali, A.; Chavanidis, K.; Soupios, P., 2024. Magnetotelluric Case Study from Ain Al-Harrah Hot Spring, Al-Lith, Saudi Arabia. Arabian Journal for Science and Engineering, 49(1), 899-912.
Awan, A. A.; Sohail, M., 2023. Determinants of Electricity Demand: An Empirical Analysis of Pakistan. Journal of Energy and Environmental Policy Options, 2(4), 72-82.
Bakar, M. A., 1955. Thermal Springs of Pakistan. In: Geological Survey of Pakistan: Quetta, 7, 1-30.
Bakar, M. A., 1965. Thermal springs of Pakistan. Pakistan Geological Survey Records, 16.
Bakht, M. S., 2000. An overview of Geothermal Resources of Pakistan. Proceedings World Geothermal Congress, 77-83.
Batayneh, A. T. 2013. The estimation and significance of Dar-Zarrouk parameters in the exploration of quality affecting the Gulf of Aqaba coastal aquifer systems. Journal of Coastal Conservation, 17, 623-635.
Bayowa, O.; Afolabi, O.; Akinluyi, F.; Oshonaiye, A.; Adelere, I.; Mudashir, A., 2023. Integrated geoelectrics and hydrogeochemistry investigation for potential groundwater contamination around a reclaimed dumpsite in Taraa, Ogbomoso, Southwestern Nigeria. International Journal of Energy and Water Resources, 7(1), 133-154.
Bobachev, C., 2002. IPI2Win: A windows software for an automatic interpretation of resistivity sounding data. Type. Thesis, Moscow State University, Moscow, Russia.
Bouaicha, F.; Dib, H.; Bouteraa, O.; Manchar, N.; Boufaa, K.; Chabour, N.; Demdoum, A., 2019. Geochemical assessment, mixing behavior and environmental impact of thermal waters in the Guelma geothermal system, Algeria. Acta Geochimica, 38, 683-702.
Chabaane, A.; Redhaounia, B.; Gabtni, H., 2017. Combined application of vertical electrical sounding and 2D electrical resistivity imaging for geothermal groundwater

characterization: Hammam Sayala hot spring case study (NW Tunisia). Journal of African Earth Sciences, 134, 292-298.

Cheon, Y.; Shin, Y. H.; Park, S.; Choi, J.-H.; Kim, D.-E.; Ko, K.; Ryoo, C.-R.; Kim, Y.-S.; Son, M., 2023. Structural architecture and late Cenozoic tectonic evolution of the Ulsan Fault Zone, SE Korea: New insights from integration of geological and geophysical data. Frontiers in Earth Science, 11, 1183329.

Dambly, M. L.; Samrock, F.; Grayver, A.; Eysteinsson, H.; Saar, M. O., 2024. Geophysical imaging of the active magmatic intrusion and geothermal reservoir formation beneath the Corbetti prospect, Main Ethiopian Rift. Geophysical Journal International, 236(3), 1764-1781.

Dávalos-Elizondo, E.; Atekwana, E. A.; Atekwana, E. A.; Tsokonombwe, G.; Laó-Dávila, D. A., 2021. Medium to low enthalpy geothermal reservoirs estimated from geothermometry and mixing models of hot springs along the Malawi Rift Zone. Geothermics, 89, 101963.

Dotsika, E.; Poutoukis, D.; Michelot, J.; Kloppmann, W., 2006. Stable isotope and chloride, boron study for tracing sources of boron contamination in groundwater: boron contents in fresh and thermal water in different areas in Greece. Water, Air, and Soil Pollution, 174, 19-32.

Escobedo, D.; Patrier, P.; Beaufort, D.; Gibert, B.; Levy, L.; Findling, N.; Mortensen, A., 2021. Contribution of the paragenetic sequence of clay minerals to re-examination of the alteration zoning in the Krafla geothermal system. Minerals, 11(9), 935.

Ewusi, A.; Attobrah, B.; Seidu, J., 2024. Estimation of aquifer transmissivity at Gushiegu and Karaga districts of Northern Ghana using Dar-Zarrouk parameters. International Journal of Energy and Water Resources, 8(1), 55-71.

Finn, C. A.; Bedrosian, P. A.; Holbrook, W. S.; Auken, E.; Bloss, B. R.; Crosbie, J., 2022. Geophysical imaging of the Yellowstone hydrothermal plumbing system. Nature, 603(7902), 643-647.

Fu, Z.; Zhang, Y.; Ji, H.; Zhang, C.; Chen, D.; Qin, Y., 2024. Characteristics of resistivity variation in deep granite and in-situ detection applications. Scientific Reports, 14(1), 6120.

Holechek, J. L.; Geli, H. M.; Sawalhah, M. N.; Valdez, R., 2022. A global assessment: can renewable energy replace fossil fuels by 2050? Sustainability, 14(8), 4792.

Iduma, R. E. O.; Uko, E. D., 2016. Dar Zarrouk Parameter as a Tool for Evaluation of Well Locations in Afikpo and Ohaozara, Southeastern Nigeria. Journal of Water Resource and Protection, 8(04), 505.

Jabrane, O.; Martínez-Pagán, P.; Martínez-Segura, M. A.; Alcalá, F. J.; El Azzab, D.; Vásconez-Maza, M. D.; Charroud, M., 2023. Integration of electrical resistivity tomography and seismic refraction tomography to investigate subsiding sinkholes in Karst areas. Water, 15(12), 2192.

Jamali, M. A.; Agheem, M. H.; Markhand, A. H.; Shaikh, S. A.; Arain, A. Y. W.; Sahito, A. G.; Memon, K. A.; Mujtaba, W. H., 2021. Exploration of Shallow Geothermal Energy Aquifers by Using Electrical Resistivity Survey in Laki Range Jamshoro district Sindh, Pakistan. International Journal of Economic and Environmental Geology, 12(1), 46-52.

Joshua, E. O.; Odeyemi, O. O.; Fawehinmi, O. O., 2011. Geoelectric investigation of the groundwater potential of Moniya Area, Ibadan. Journal of Geology and Mining Research, 3(3), 54-62.

Junaid, M.; Abdullah, R. A.; Sa'ari, R.; Ali, W.; Rehman, H.; Alel, M. N. A.; Ghani, U., 2021 2D Electrical Resistivity Tomography an advance and expeditious exploration technique for current challenges to mineral industry. Journal of Himalayan Earth Science, 54(1), 11-32.

Kanwal, S.; Mehran, M. T.; Hassan, M.; Anwar, M.; Naqvi, S. R.; Khoja, A. H., 2022. An integrated future approach for the energy security of Pakistan: Replacement of fossil fuels with syngas for better environment and socio-economic development. Renewable and Sustainable Energy Reviews, 156, 111978.

Kaur, S.; Yadav, J. S.; Bhambri, R.; Sain, K.; Tiwari, S. K., 2023. Assessment of geothermal potential of Kumaun Himalaya: A perspective for harnessing

green energy. Renewable Energy, 212, 940-952.

Kazakis, N.; Vargemezis, G.; Voudouris, K. S., 2016. Estimation of hydraulic parameters in a complex porous aquifer system using geoelectrical methods. Science Total Environment, 550, 742-750.

Khan, R.; Shah, S. H.; Khan, N. A., 1999. Investigation of the Geothermal Springs of the Tatta Pani Area District Kotli Azad Jammu & Kashmir. In Geological Survey of Pakistan Quetta, 701.

Komori, S.; Takakura, S.; Mitsuhata, Y.; Yokota, T.; Uchida, T.; Makino, M.; Kato, Y.; Yamamoto, K., 2024. Three-dimensional resistivity structure in Toya caldera region, Southwest Hokkaido, Japan—Constraints on magmatic and geothermal activities. Geophysics, 89(1), B31-B50.

Krzyżak, A. T.; Habina-Skrzyniarz, I.; Machowski, G.; Mazur, W., 2020. Overcoming the barriers to the exploration of nanoporous shales porosity. Microporous and Mesoporous Materials, 298, 110003.

Ladygin, V.; Frolova, Y. V.; Rychagov, S., 2014. The alteration of effusive rocks due to acidic leaching by shallow thermal waters: The Baranskii geothermal system, Iturup Island. Journal of Volcanology and Seismology, 8, 17-33.

Loke, M. H.; Rucker, D.; Chambers, J.; Wilkinson, P.; Kuras, O., 2020. Electrical resistivity surveys and data interpretation. In: Encyclopedia of solid earth geophysics, Springer: pp 1-6.

Lund, J. W.; Toth, A. N., 2021. Direct utilization of geothermal energy 2020 worldwide review. Geothermics, 90, 101915.

Mahmud, S.; Hamza, S.; Irfan, M.; Huda, S. N.-u.; Burke, F.; Qadir, A., 2022. Investigation of groundwater resources using electrical resistivity sounding and Dar Zarrouk parameters for Uthal Balochistan, Pakistan. Groundwater for Sustainable Development, 17, 100738.

Maillet, R., 1947. The fundamental equations of electrical prospecting. Geophysics, 12(4), 529-556.

Markússon, S. H.; Stefánsson, A., 2011. Geothermal surface alteration of basalts, Krýsuvík Iceland—Alteration mineralogy, water chemistry and the effects of acid supply on the alteration process. Journal of Volcanology and Geothermal Research, 206(1-2), 46-59.

Mohammed, M. A.; Szabó, N. P.; Alao, J. O.; Szűcs, P., 2024. Geophysical characterization of groundwater aquifers in the Western Debrecen area, Hungary: insights from gravity, magnetotelluric, and electrical resistivity tomography. Sustainable Water Resources Management, 10(2), 67.

Mughal, M. N.; Khan, R.; Hussain, A., 2004. Geological Map of the Kotli Area, part of Kotli and Sudhonti districts AJK, 43 G/14. In: Geological Survey of Pakistan Quetta.

Nastasi, B.; Markovska, N.; Puksec, T.; Duić, N.; Foley, A., 2022. Renewable and sustainable energy challenges to face for the achievement of Sustainable Development Goals. In: Elsevier: 157, 112071.

Navarro, A.; Font, X.; Viladevall, M., 2011. Geochemistry and groundwater contamination in the La Selva geothermal system (Girona, Northeast Spain). Geothermics, 40(4), 275-285.

Nieto, I. M.; Martín, A. F.; Blázquez, C. S.; Aguilera, D. G.; García, P. C.; Vasco, E. F.; García, J. C., 2019. Use of 3D electrical resistivity tomography to improve the design of low enthalpy geothermal systems. Geothermics, 79, 1-13.

Olabi, A. G.; Mahmoud, M.; Soudan, B.; Wilberforce, T.; Ramadan, M., 2020. Geothermal based hybrid energy systems, toward eco-friendly energy approaches. Renewable Energy, 147, 2003-2012.

Oyeyemi, K. D.; Abuka-Joshua, J.; Rotimi, O. J.; Dieppois, B.; Gomo, M.; Olaojo, A. A.; Falae, P. O.; Metwaly, M., 2023. Geoelectrical Characterization of Coastal Aquifers in Agbado-Ijaye, Lagos, Southwestern Nigeria; Implications for Groundwater Resources Sustainability. Sustainability, 15(4), 3538.

Pavić, M.; Kosović, I.; Pola, M.; Urumović, K.; Briški, M.; Borović, S., 2023. Multidisciplinary Research of Thermal Springs Area in Topusko (Croatia). Sustainability, 15(6), 5498.

Rashid, M. u.; Anwar, S., 2018. Subsurface Mapping of Geothermal Hot Spring at Tattapani Kotli, Azad Jammu and Kashmir

using Vertical Electrical Sounding Publication Directorate GSP, Quetta, 1029, 1-30.

Rashid, M. u.; Ahmed, W.; Anwar, S.; Abbas, S. A.; Khan, S.; Ahmed, K. A., 2018. Geo-electrical survey for the appraisal of groundwater resource in Siwalik group: a case study of Khrick Rawlakot, Azad Kashmir. Journal of Himalayan Earth Sciences, 51(1), 44-60.

Rashid, M. u.; Ahmed, W.; Anwar, S.; Abbas, S. A.; Waseem, M.; Khan, S., 2017. Groundwater resource characterization using geo-electrical survey: a case study of Rawlakot, Azad Jammu and Kashmir. Journal of Himalayan Earth Sciences, 50(2), 125-136.

Raza, M. A.; Khatri, K. L.; Israr, A.; Haque, M. I. U.; Ahmed, M.; Rafique, K.; Saand, A. S., 2022. Energy demand and production forecasting in Pakistan. Energy Strategy Reviews, 39, 100788.

Rosado-Fuentes, A.; Arciniega-Ceballos, A.; Hernández-Quintero, E.; Arango-Galván, C.; Salas-Corrales, J. L.; Mendo-Pérez, G., 2023. Mapping near-surface structures in a geophysical test site using magnetic and electromagnetic induction gradients. Journal of Applied Geophysics, 215, 105123.

Shah, S. H.; Abbas, Q.; Tariq, M.; Mehmood, Z., 2007. Geological Map of Tatta Pani Coal Field, District Kotli, Azad Kashmir. Publication Directorate GSP, Quetta, Geological Map Series No.2.

Shahid, M.; Ullah, K.; Imran, K.; Mahmood, I.; Mahmood, A., 2020. Electricity supply pathways based on renewable resources: A sustainable energy future for Pakistan. Journal of Cleaner Production, 263, 121511.

Shuja, T.; Sheikh, M., 1983. A study of geothermal resources of Gilgit and Hunza agencies, northern Pakistan. Geological Survey of Pakistan Info Rel, 179, 22.

Shuja, T. A., 1986. Geothermal areas in Pakistan. Geothermics, 15(5), 719-723.

Shuja, T. A., 1988. Small geothermal resources in Pakistan. Geothermics, 17(2), 461-464.

Shuja, T. A.; Khan, N. A., 1984. Prospects of geothermal energy in Pakistan. In Geological Survey of Pakistan Quertta, Geological Survey of Pakistan Quetta, 242.

Singh, S.; Gautam, P. K.; Bagchi, D.; Singh, S.; Kumar, S.; Kannaujiya, S., 2021. 2D electrical resistivity imaging for geothermal groundwater characterization and rejuvenation of the Gaurikund hot spring in the Main Central Thrust (MCT) zone of the Garhwal Himalaya, Uttrakhand, India. Groundwater for Sustainable Development, 15, 100686.

Telford, W. M.; Geldart, L. P.; Sheriff, R. E., 1990. Applied geophysics: Cambridge University Press: Cambridge, 1.

Thakur, V.; Jayangondaperumal, R.; Malik, M., 2010. Redefining Medlicott–Wadia's main boundary fault from Jhelum to Yamuna: An active fault strand of the main boundary thrust in northwest Himalaya. Tectonophysics, 489(1), 29-42.

Todaka, N.; Shuja, T. A.; Jamiluddin, S.; Khan, N. A.; Pasha, M. a.; Iqbal, M., 1988. A preliminary Study of Geothermal Energy Resources of Pakistan. In: Geological Survey of Pakistan, 407, 1-55.

Todaka, N.; Shuja, T. A.; Jamiluddin, S.; Khan, N. A.; Pasha, M. A.; Iqbal, M., 1988. A preliminary Study of Geothermal Energy Resources of Pakistan. In: Geological Survey of Pakistan, 407.

Wang, B.; Zhou, X.; Li, J.; Zhang, Y.; Shen, J.; Zhong, J.; Bao, Z., 2024. Hydrogeochemical and geothermal features of thermal springs along the Ganzi-Yushu fault, eastern Tibetan Plateau and its geological implications. Applied Geochemistry, 161, 105898.

Wang, J.; Gao, S.; Wang, J.; Li, L.; Gong, X.; Su, J., 2024. Application of integrated geophysical techniques in geothermal exploration in Binhai County, Jiangsu Province. Deep Underground Science and Engineering.

Yang, Y.; Cao, Q.; Fang, C.; Zhu, C., 2023. Characteristics of geothermal field and evaluation of geothermal resource potential in the Yingjiang basin. Energy Geoscience, 100210.

Yang, Y.; Xiong, B.; Peng, S.; Chen, H.; Zhang, T.; Liu, L., 2022. Geothermal exploration using numerical simulation and a comprehensive electromagnetic method. Petroleum Science and Technology, 1-25.

Yanis, M.; Ismail, N.; Abdullah, F., 2022. Shallow Structure fault and fracture

mapping in Jaboi Volcano, Indonesia, using VLF–EM and electrical resistivity methods. Natural Resources Research, 1-18.

Zaigham, N. A.; Nayyar, Z. A., 2010. Renewable hot dry rock geothermal energy source and its potential in Pakistan. Renewable and Sustainable Energy Reviews, 14(3), 1124-1129.

Zaigham, N. A.; Nayyar, Z. A.; Hisamuddin, N., 2009. Review of geothermal energy resources in Pakistan. Renewable and Sustainable Energy Reviews, 13(1), 223-232.

Zhou, X.; Zhuo, L.; Wu, Y.; Tao, G.; Ma, J.; Jiang, Z.; Sui, L.; Wang, Y.; Wang, C.; Cui, J., 2023. Origin of some hot springs as conceptual geothermal models. Journal of Hydrology, 624, 129927.

Zhu, Y.-Q.; Li, D.-Q.; Zhang, Q.-X.; Zhang, X.; Liu, Z.-J.; Wang, J.-H., 2022. Characteristics of geothermal resource in Qiabuqia, Gonghe Basin: Evidence from high precision resistivity data. Ore Geology Reviews, 105053.